RESEARCH ARTICLE

Enhanced RhoA signalling stabilizes E-cadherin in migrating epithelial monolayers

Shafali Gupta[1], Kinga Duszyc[1], Suzie Verma[1], Srikanth Budnar[1,*], Xuan Liang[1,‡], Guillermo A. Gomez[1,§], Philippe Marcq[2], Ivar Noordstra[1] and Alpha S. Yap[1,¶]

ABSTRACT

Epithelia migrate as physically coherent populations of cells. Previous studies have revealed that mechanical stress accumulates in these cellular layers as they move. These stresses are characteristically tensile in nature and have often been inferred to arise when moving cells pull upon the cell–cell adhesions that hold them together. We now report that epithelial tension at adherens junctions between migrating cells also increases due to an increase in RhoA-mediated junctional contractility. We found that active RhoA levels were stimulated by p114 RhoGEF (also known as ARHGEF18) at the junctions between migrating MCF-7 monolayers, and this was accompanied by increased levels of actomyosin and mechanical tension. Applying a strategy to restore active RhoA specifically at adherens junctions by manipulating its scaffold, anillin, we found that this junctional RhoA signal was necessary to stabilize junctional E-cadherin (CDH1) during epithelial migration and promoted orderly collective movement. We suggest that stabilization of E-cadherin by RhoA serves to increase cell–cell adhesion to protect against the mechanical stresses of migration.

This article has an associated First Person interview with the first author of the paper.

KEY WORDS: Epithelial migration, Adherens junction, E-cadherin, RhoA, Contractility

INTRODUCTION

Cell migration is a complex mechanical process. Cells translocate by applying physical forces onto their environment, elements of the extracellular matrix (ECM) or other, adjacent cells. In turn, forces can be applied to migrating cells. This is exemplified by the collective migration of epithelia and endothelia, which characteristically move as coherent cell populations, whose constituent cells are physically linked together by cell–cell adhesions (Friedl and Gilmour, 2009; Friedl and Mayor, 2017). Studies using two-dimensional epithelial monolayers have shown that mechanical stresses build up within the cellular layers as they migrate (Reffay et al., 2014; Tambe et al., 2011; Trepat et al., 2009). These stresses have been inferred to increase at cell–cell adhesions. As cells in these experiments were typically crawling on ECM-based substrata via integrin adhesions, the build-up in cellular stress has been thought to reflect the transmission of traction forces through the cell to cell–cell junctions (Trepat and Fredberg, 2011). One simple model is that mechanical stresses at cell–cell adhesions would increase passively as migrating cells pull upon one another. Cadherin-based adherens junctions (AJs) are coupled to the F-actin cytoskeleton by intermediary proteins, such as α-catenin, vinculin and myosin VI (MYO6), that can bind directly to actin filaments (Lecuit and Yap, 2015). This physical coupling provides a way for traction forces to be transmitted through the actomyosin cytoskeleton to AJs.

Cadherin adhesions can also actively regulate their associated cytoskeleton by recruiting actin regulators and signalling molecules that target the cytoskeleton (Lecuit and Yap, 2015). In particular, AJs in interphase epithelia are prominent sites of signalling by the RhoA GTPase. RhoA at AJs is activated by a number of upstream pathways, anchored by distinct guanine-nucleotide-exchange factors (GEFs) (Acharya et al., 2018; Garcia De Las Bayonas et al., 2019; Ratheesh et al., 2012), and RhoA signals to promote formin-based actin assembly and non-muscle myosin II (NMII) recruitment at AJs (Acharya et al., 2017; Cavanaugh et al., 2020; Curran et al., 2017; Ratheesh et al., 2012). In this report, we show that RhoA signalling increases at AJs during epithelial migration, revealing that upregulation of active force generation at AJs contributes to the build-up of tension at these cell–cell junctions. We further show that RhoA at AJs enhances E-cadherin (also known as CDH1) stability during epithelial migration.

RESULTS

AJ contractility increases during epithelial migration

MCF-7 mammary epithelial cells, which establish robust AJs (Smutny et al., 2010), were grown to confluence in silicone moulds that were then removed to allow the cells to migrate. Over the 12 h course of our experiments, 12–15 rows of cells moved into the open space created by the mould. Lamellipodia were evident throughout the motile population, both at the leading margins of the sheet and also as cryptic lamellipodia within the moving sheet (Fig. S1A, Movie 1), consistent with the notion that this moving population consisted of individually locomotile cells connected together by AJs. Immunostaining for E-cadherin in the first ten rows of cells from the migrating front confirmed that the cells had assembled AJs before the assays began, and these were preserved in the migrating sheets (Fig. S1B).

Tensile stresses in migrating epithelia have often been characterized using inference techniques applied to traction force data (Tambe et al., 2011). To test whether similar phenomena applied

[1]Division of Cell and Developmental Biology, Institute for Molecular Bioscience, The University of Queensland, St. Lucia, Brisbane 4072, Australia. [2]Physique et Mécanique des Milieux Hétérogènes, CNRS, ESPCI Paris, PSL University, Sorbonne Université, Université de Paris, F-75005 Paris, France.
*Present address: CSL Ltd, Bio21 Institute, Melbourne, Victoria 3052, Australia.
‡Present address: Department of Physiology, Development and Neuroscience, University of Cambridge, Downing Street, Cambridge CB2 3DY, UK. §Present address: Centre for Cancer Biology, SA Pathology and the University of South Australia, Adelaide, SA 5001, Australia.

¶Author for correspondence (a.yap@uq.edu.au)

K.D., 0000-0003-2478-2089; S.B., 0000-0002-8951-9081; P.M., 0000-0002-3232-9156; I.N., 0000-0001-5381-8795; A.S.Y., 0000-0002-1038-8956

in our system, we performed traction force microscopy as MCF-7 cells migrated upon polydimethylsiloxane (PDMS) substrata and inferred stresses in the cellular layer using Bayesian inversion stress microscopy (BISM; Nier et al., 2016; Ollech et al., 2020) (see Materials and Methods for details). Stresses were predominantly tensile when the MCF-7 monolayers were examined just after the moulds were removed (which we term 'premigratory'), indicating that the cells were not over-confluent or compressed before the start of the experiment (Fig. 1A). These tensile stresses increased with migration (Fig. 1B; Movie 2). Thus, migrating MCF-7 cells showed increases in monolayer tension similar to what has previously been reported for other types of epithelial cells.

To more specifically evaluate changes in junctional tension in migrating cells, we identified AJs by expressing E-cadherin–mCherry and measured their initial recoil after being cut by laser ablation (Ratheesh et al., 2012). Basal recoil was evident at AJs in premigratory monolayers, and this increased with migration (Figs 1C and 6D,E; Fig. S6), consistent with an increase in tension within the AJs between migrating cells. To assess whether molecular-level tension changed at the AJs, we then immunostained cells for the α-18 epitope of α-catenin (CTNNA1), a cryptic site that is revealed when tension is applied (Yonemura et al., 2010). Monoclonal antibody staining for α-18, expressed as a ratio of α-18 to total α-catenin, increased in migrating monolayers (Fig. 1D; Fig. S1C). Taken together, these findings imply that tension increases at AJs of migrating MCF-7 cells.

This observed increase in AJ tension could have occurred if AJs passively resisted forces of migration being transmitted from elsewhere in the cells and/or if contractility at AJs was itself enhanced. We examined this further by evaluating actomyosin at AJs. Phalloidin staining revealed that levels of cortical F-actin increased at the cell–cell contacts (Fig. 1E,H; Fig. S1D). MCF-7 cells express all three mammalian NMII paralogs (Smutny et al., 2010), and antibodies were available that effectively recognized NMIIA and NMIIB (which contain the MYH9 and MYH10 heavy chains, respectively) (Fig. 1F,G; Fig. S1D). Indeed, quantitative immunofluorescence showed that both NMIIA and NMIIB increased at AJs in migrating cells (Fig. 1I,J). Overall, this local increase in actomyosin could potentially have contributed to increasing tension at AJs during collective migration.

RhoA signalling is upregulated at AJs during collective epithelial migration

To explore whether contractility was actively upregulated at AJs between migrating cells, we focused on the RhoA GTPase, a canonical regulator of cellular actomyosin that is also active at AJs (Priya et al., 2013; Ratheesh et al., 2012). We therefore investigated whether junctional RhoA is altered during MCF-7 sheet migration. To identify the sites of RhoA signalling in collectively-migrating MCF-7 cells, we expressed AHPH, a location biosensor that identifies active, GTP-loaded RhoA (Piekny and Glotzer, 2008; Priya et al., 2015). AJs were prominent sites of GTP-RhoA in premigratory monolayers (Fig. 2A, image intensity in the images presented was reduced to avoid saturation; Fig. S2A). Strikingly, AHPH levels at junctions increased significantly when cells began to move (Fig. 2A,B; Movie 3). To quantify the changes in AHPH signal, we divided the cell population into three zones (Fig. S2C) consisting of cell rows 1–5 (zone 1), rows 6–10 (zone 2) and rows 11–16 (zone 3) from the front of the moving population. AHPH levels at AJs increased with time in all these zones (Fig. 2B), but the increase was most evident in the cells closest to the front (zone 1), which were the first to begin moving. AHPH was also evident in the

free lamellipodia of the leader cells (Fig. S2B), but this did not increase with time (Fig. 2C), in contrast to the junctional signal (Fig. 2C).

The increase in junctional RhoA signalling was confirmed using an intramolecular fluorescence resonance energy transfer (FRET)-based RhoA-activity sensor (Fig. S2D), where energy exchange increases upon activation of the RhoA moiety of the reporter. Quantitation of the junctional FRET signal in zone 1 (Fig. S2C) showed that RhoA activation was increased in this region of the migrating monolayer (Fig. S2D). The FRET reporter also revealed an increase in signal away from the junctions, which may correspond to a medial–apical pool of RhoA. Taken together, these findings indicate that RhoA signalling is upregulated at AJs when MCF-7 cells migrate.

Next, we tested this observation in a transgenic zebrafish line expressing GFP–AHPH [tg(krt4:GFP-AHPH)^{uqay2}] (Duszyc et al., 2021) during epiboly, a form of collective migration in the early vertebrate embryo (Bruce and Heisenberg, 2020). Embryos expressing GFP–AHPH showed AHPH staining at their medial–apical cortex as well as at cell–cell junctions. During early epiboly, AHPH was first evident in puncta at the medial–apical surface of the cells, then became prominent at junctions by 50% epiboly, where it subsequently increased (Fig. 2D,E; Movie 4). This increase in junctional AHPH was most evident in the cells in the enveloping layer that move towards the vegetal pole to lead the migratory process (zone I in Fig. 2D,E), although it was also seen in cells closer to the animal pole (zone II in Fig. 2E). Therefore, the upregulation of junctional RhoA signalling may be a general feature of collective epithelial migration, which could contribute to enhancing contractile tension at AJs.

Junctional GTP-RhoA levels increase before monolayer tension

We then sought to compare how spatial patterns of mechanical stress and RhoA signalling evolved as epithelia migrated. For this, we grew MCF-7 cells expressing GFP–AHPH on PDMS substrata and performed simultaneous evaluation of monolayer stress (using BISM and traction force microscopy) and junctional AHPH (Fig. 3). This showed, broadly, that monolayer stresses increased in the regions that also showed an increase in junctional GTP-RhoA (Fig. 3A). We then quantitated these changes by comparing the mean tensile stress (Fig. 3B) and the average levels of AHPH at AJs (Fig. 3C) within the fields of view. Both junctional GTP-RhoA and monolayer stress increased as the cells migrated, although junctional GTP-RhoA levels were lower in these cells grown on soft PDMS substrata (Fig. 3C) than when cells migrated on glass. Interestingly, junctional GTP-RhoA levels increased more quickly and earlier than the levels of monolayer stress (Fig. 3B,C). This suggests that the rise in junctional RhoA might contribute to the increase in monolayer tension.

p114 RhoGEF participates in activating junctional RhoA during migration

A number of GEFs have been reported to stimulate RhoA at AJs (Garcia De Las Bayonas et al., 2019). In mammalian epithelial cells, these include Ect2, which appears to support steady-state RhoA signalling at interphase AJs (Ratheesh et al., 2012), and p114 RhoGEF (also known as ARHGEF18), which can increase junctional RhoA activity when tensile forces are applied to epithelia (Acharya et al., 2018). We focused on p114 RhoGEF, which showed faint immunostaining at AJs in premigratory MCF-7 monolayers, and increased with migration (Fig. 4A,B). Total cellular levels of
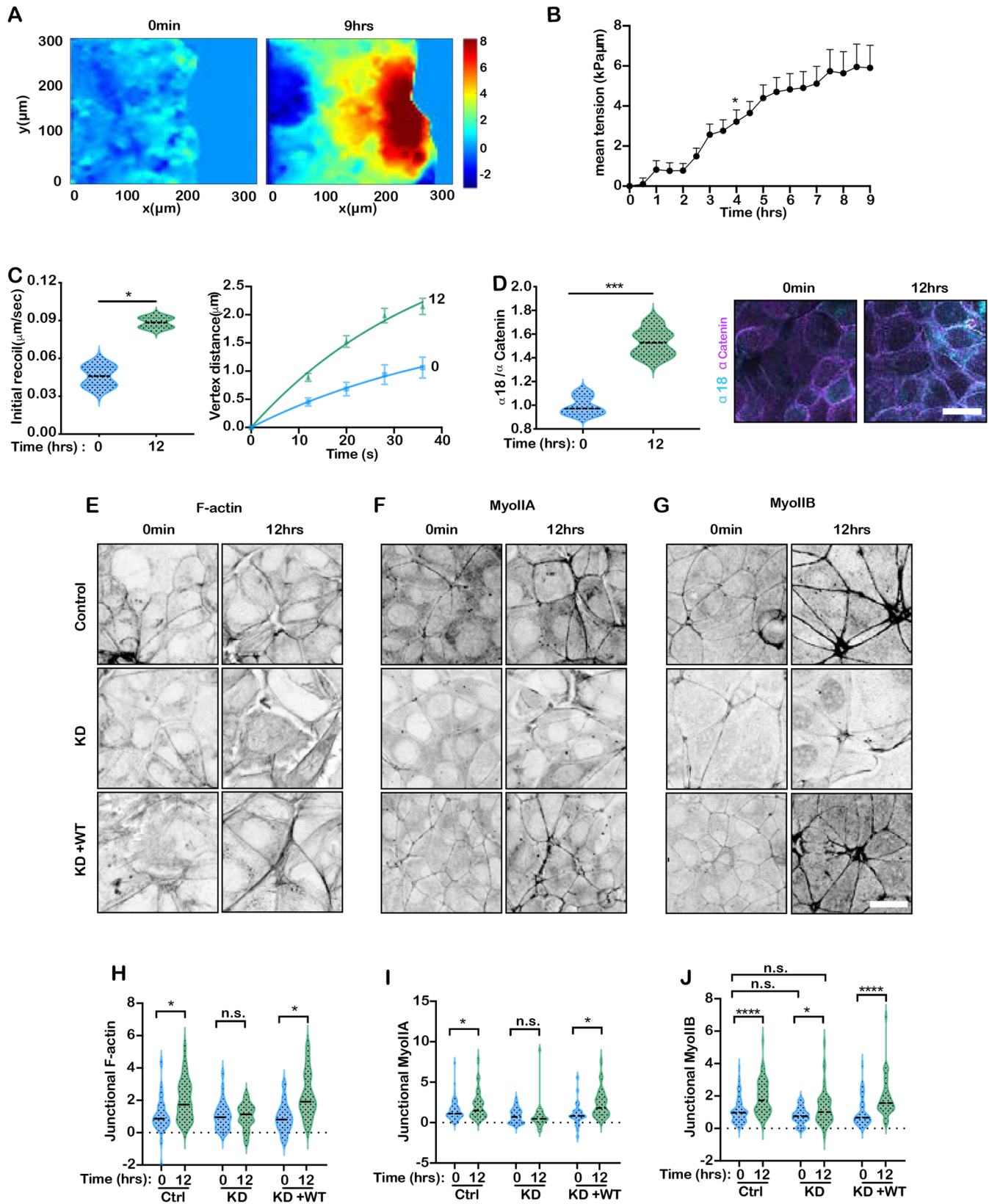
Fig. 1. See next page for legend.

p114 RhoGEF did not change (Fig. 4C), suggesting that the increased junctional staining was due to enhanced recruitment. In contrast, the levels of Ect2 at AJs did not change upon migration (Fig. S3A).

Next, we asked whether p114 RhoGEF RNAi (Fig. S3B) affected RhoA signalling at AJs during epithelial migration. p114 RhoGEF depletion did not alter baseline levels of junctional GTP-RhoA, but it prevented GTP-RhoA from increasing when the cells migrated

Fig. 1. AJ tension increases in migrating epithelial cells. (A,B) Stress in MCF-7 epithelial monolayers before (0 h) and after 9 h of migration, calculated using BISM. Representative stress maps (A) and quantification of mean tension within the field of view (B). Positive values are tensile. (C) AJ tension inferred from recoil velocity after laser ablation of AJs. Initial recoil velocities (left) and recoil curves (right) for cells at 0 h and 12 h of migration are shown. (D) Tension at the cadherin–catenin complex inferred from immunostaining for α-18 at AJs using a monoclonal antibody (normalized to α-catenin staining). Quantification (left) and representative images (right) for cells at 0 h and 12 h of migration are shown. (E–J) Junctional F-actin (E,H), NMIIA (MyoII) (F,I) and NMIIB (MyoIIB) (G,J) in migrating MCF-7 cells expressing control shRNA, anillin shRNA (KD) or anillin shRNA reconstituted with full-length GFP–anillin (KD+WT). Representative images (E–G) and quantification of staining intensity (H–J) are shown. Data for C–J were collected from within the first seven rows of cells. In the violin plots, dashed black lines indicate the mean. Data in B and C are mean±s.e.m. n=3 independent experiments (for C–J, each independent experiment has 18–22 technical replicates). n.s., not significant; *P<0.05; ***P<0.001; ****P<0.0009. Two-tailed, unpaired t-test (C,D) or one-way ANOVA with Dunnett's multiple comparisons test (B,H,I,J). Scale bars: 20 μm.

(Fig. 4D,E). Consistent with this, junctional NMIIA levels did not increase when p114 RhoGEF-knockdown (KD) cells migrated (Fig. 4F,G). In contrast, depleting LARG (also known as ARHGEF12; Fig. S3C), another mechanically activated RhoGEF (Guilluy et al., 2011), did not prevent either GTP-RhoA (Fig. 4D,E) or NMIIA (Fig. 4F,G) from increasing at AJs during migration. This implies that p114 RhoGEF is critically responsible for enhancing RhoA at AJs when MCF-7 cells migrate. As p114 RhoGEF can activate RhoA when tension is applied to AJs (Acharya et al., 2018), it is possible that during epithelial migration it responds to tugging forces that moving cells apply to one another. p114 RhoGEF would then provide a mechanism for active junctional contractility to be elicited when traction forces are transmitted to AJs.

Anillin depletion prevents the upregulation of junctional RhoA

Our end goal was to understand how RhoA might affect AJ function in migrating cells. However, manipulation of p114 RhoGEF presented interpretative complexities, because this GEF also activates RhoA at other sites within cells (Kelly et al., 2007), including epithelial tight junctions (Terry et al., 2011). To focus on the impact of RhoA at AJs, we therefore required an alternative approach that would allow us to manipulate it specifically at these junctions.

For this purpose, we exploited our recent discovery that the cytoskeletal protein anillin (Fig. 5A) is a kinetic scaffold for GTP-RhoA that increases GTP-RhoA dwell time to enhance RhoA cortical signalling (Budnar et al., 2019). Anillin localizes to AJs (Fig. S4A,B) (Budnar et al., 2019) and, indeed, increased at AJs in migrating cells (Fig. S4C,D). Depleting anillin using RNAi (Fig. S4E) reduced junctional GTP-RhoA in premigratory monolayers (Fig. 5B,C), as we have observed previously (Budnar et al., 2019). It should be noted that although AHPH is derived from the C terminus of anillin, it is not affected by manipulation of anillin levels (Budnar et al., 2019).

Strikingly, although anillin-KD cells retained contact with one another as they migrated (Fig. 5D), they did not upregulate GTP-RhoA at their junctions (Fig. 5B,C). Consistent with this, anillin KD also specifically prevented F-actin (Fig. 1E,H) and NMII levels (Fig. 1F,G,I,J) from increasing at the AJs of migrating cells. This suggests that anillin is necessary for junctional RhoA to be upregulated during epithelial migration. However, anillin is found at other parts of the cell cortex and, indeed, anillin KD also reduced GTP-RhoA levels in the lamellae of leader cells (Fig. S2B).

Therefore, to selectively manipulate RhoA at AJs, we reconstituted anillin-KD cells by expression of a chimeric protein consisting of the anillin homology (AH) domain fused to α-catenin (AH–α-catenin; Budnar et al., 2019), which targeted the protein to AJs (Fig. 5A; Fig. S5). The AH domain is responsible for kinetic scaffolding of GTP-RhoA, so we reasoned that this strategy would restore RhoA activity selectively at AJs. Indeed, expression of AH–α-catenin restored the capacity for migrating KD cells to upregulate GTP-RhoA at their junctions, despite anillin being otherwise depleted in the cells (Fig. 5B,C), but this did not occur with the AH^{DM}–α-catenin mutant, which cannot stabilize GTP-RhoA because it lacks key residues needed to bind GTP-RhoA (Fig. 5A–C; Budnar et al., 2019). Combining anillin KD with AH–α-catenin reconstitution thus provided a strategy to selectively interrogate the impact of junctional RhoA signalling on AJs in epithelial migration.

Upregulation of RhoA stabilizes E-cadherin in migrating monolayers

As RhoA signalling stabilizes E-cadherin at AJs (Priya et al., 2013; Ratheesh et al., 2012), we first asked whether the increased junctional RhoA observed in migrating MCF-7 cells might affect E-cadherin at their junctions. As previously reported (Budnar et al., 2019), anillin KD reduced E-cadherin levels at zonulae adherente in premigratory monolayers (Fig. 5D), although total E-cadherin levels were not altered (Fig. S4F). This is consistent with previously published evidence that RhoA-driven junctional tension stabilizes E-cadherin at the specialized apical–lateral zone of the zonula adherens (Priya et al., 2013; Ratheesh et al., 2012). Moreover, while E-cadherin levels at junctions increased in migrating cells, this was selectively reduced by anillin KD (Fig. 5D,E).

To better understand why E-cadherin levels at junctions were altered during migration, we used fluorescence recovery after photobleaching (FRAP) assays to measure the turnover of E-cadherin–mCherry. Control cells stabilized E-cadherin–mCherry as they migrated, as reflected in an increased immobile fraction. Strikingly, E-cadherin was more dynamic in premigratory anillin-KD cells, consistent with the lower levels evident by immunostaining, and this failed to become more stable upon migration. Importantly, stabilization of E-cadherin during migration was restored to anillin-KD cells by expression of AH–α-catenin. The premigratory immobile fraction was increased, compared with that in anillin-KD cells, and stabilized further upon migration (Fig. 5F,G). This indicates that E-cadherin is stabilized as a specific consequence of RhoA signalling at AJs. Taken together, these findings indicate that the junctional RhoA signalling that increases in migrating MCF-7 monolayers enhances the stability of E-cadherin in these collectively moving cells.

RhoA at AJs upregulates epithelial tension during migration

We then used our anillin manipulation strategy to test the hypothesis that junctional RhoA signalling contributes to the increase in epithelial tension that we observed in migrating monolayers. First, we evaluated how monolayer stress was affected during migration. The increase in tensile monolayer stress that occurred as monolayers migrated was substantially abrogated in anillin-KD cells, an effect that was reversed when we expressed AH–α-catenin to selectively restore GTP-RhoA at the AJs (Fig. 6A–C). We then measured junctional recoil after laser ablation, to test how tension at AJs might be altered. Consistent with the BISM data, junctional recoil failed to increase when anillin-KD cells migrated, compared with recoil of either control cells or anillin-KD cells reconstituted with AH–α-catenin (Fig. 6D,E; Fig. S6). Taken together, these results establish
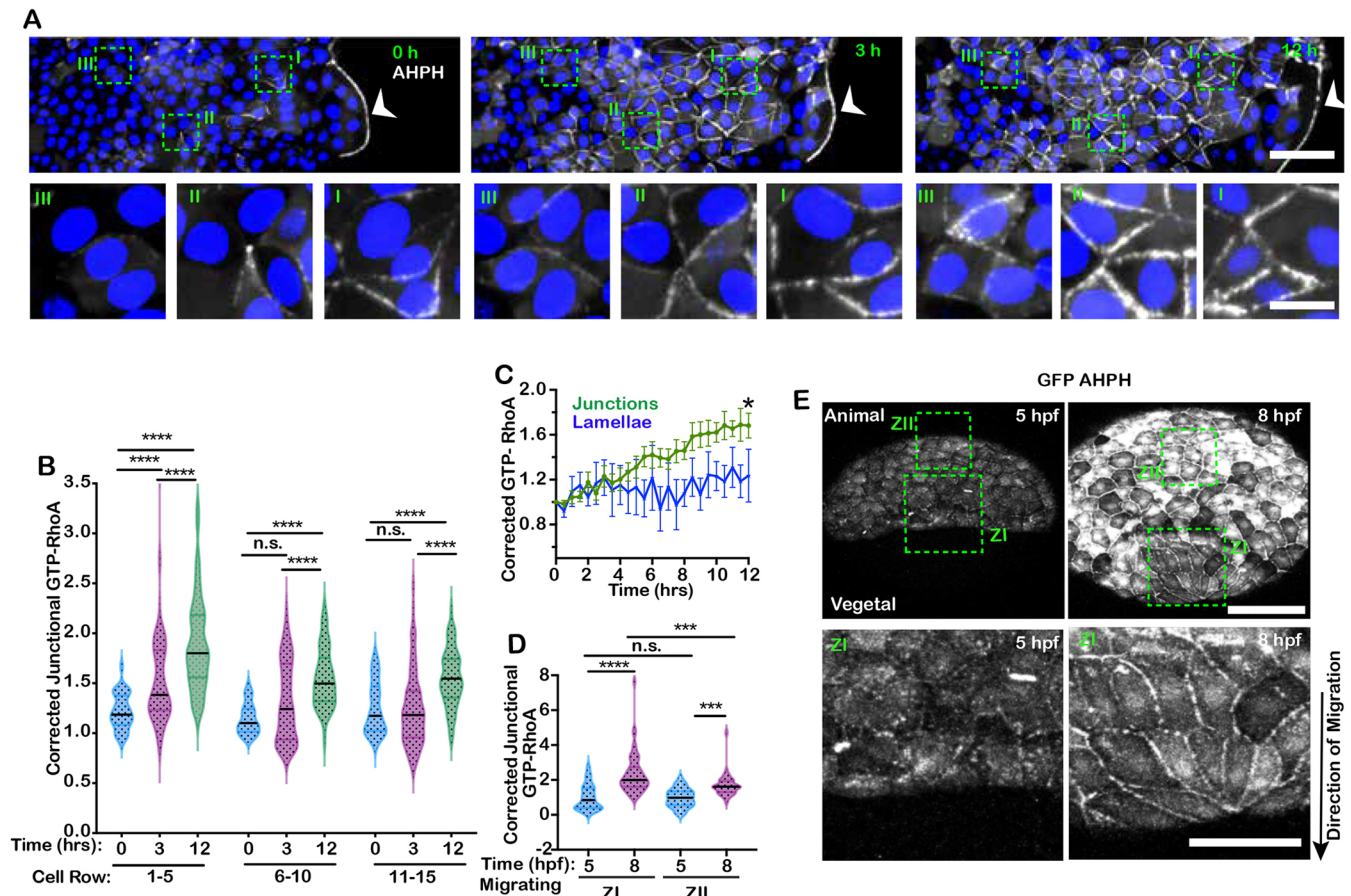
Fig. 2. RhoA signalling is upregulated at the AJs of migrating epithelial cells. (A–E) GTP-RhoA was detected using the AHPH location biosensor (GFP–AHPH) in MCF-7 cells (A–C) and zebrafish embryos (D,E). (A) Representative images of GFP–AHPH in migrating MCF-7 monolayers at the indicated time points. Dashed boxes indicate different zones of a migrating monolayer shown in magnified images beneath (I, cell rows 1–5; II, cell rows 6–10; III, cell rows 11–15). Arrowhead indicates the AHPH localisation in the lamellae. Nuclei are stained with Hoechst 33342 dye. (B) Quantification of junctional GFP–AHPH (corrected for cytosolic expression in each cell) at different zones of migrating monolayers. (C) Change in junctional GFP–AHPH at the lamellae of leader cells. (D,E) GFP–AHPH during epiboly in $tg(krt4:GFP-AHPH)^{uqay2}$ zebrafish embryos at 5 and 8 h post fertilization (hpf). Quantification of junctional GFP–AHPH (D, corrected for cytosolic expression) and representative images (E) are shown. Dashed boxes show different zones of the migrating monolayer. Zone I (ZI) is an enveloping layer close to the vegetal pole of the embryo, zone II (ZII) is at the animal pole. Magnified views of the ZI regions are shown beneath. The arrow marks the direction of migration during epiboly. In B and D, black lines show the mean. Data in C are mean±s.e.m. n=3 independent experiments (for B and C, each independent experiment contained 18–22 technical replicates). n.s., not significant; *P<0.05; ***P<0.001; ****P<0.0009. One-way ANOVA with Dunnett's multiple comparisons test. Scale bars: 100 µm (A, top panel), 20 µm (A, bottom panel) and 25 µm (E).

that AJ tension increases during epithelial migration in response to junctional RhoA signalling, as well as any stresses that may be transmitted from locomotor interactions with the cell substrate.

Upregulation of junctional RhoA promotes orderly epithelial migration

Finally, we asked how RhoA signalling at AJs might influence the migratory behaviour of MCF-7 cells. For this, we tracked cells within the moving population (first 12–15 rows of cells) by using time-lapse imaging to monitor nuclei labelled with Hoechst 33342 dye. As shown in Fig. 7A, cells characteristically moved towards the open space of these artificial wound assays (i.e. approximately orthogonal to the leading margin of the monolayer). Surprisingly, the speed of cell migration was increased in anillin-KD cells and this was restored by expression of AH–α-catenin (Fig. 7B). Furthermore, anillin-KD cells appeared to move in a less organized fashion than controls (Fig. 7A). To quantitate this, we projected the tracks of each migrating cell over the 12 h period of observation and counted the number of times cell tracks crossed one another. Our interpretation was that cells would cross tracks

minimally if collective migration was perfectly orderly, whereas an increase in track crossing would reflect a loss of orderly movement within the population. Indeed, anillin-KD cells showed an increase in the number of crossed tracks, compared with those of control cells or anillin-KD cells rescued with AH–α-catenin (Fig. 7C). Taken together, these results suggest that junctional RhoA signalling might serve to promote orderly collective migration and restrain the speed of cell locomotion. This was supported by analysis of p114 RhoGEF-KD cells, which also showed an increase in cell speed (Fig. 7B) and in the frequency of track crossing (Fig. 7C).

DISCUSSION

Taken together, our experiments reveal that RhoA signalling contributes to the increase in tensile stress that accompanies collective epithelial migration (Reffay et al., 2014; Tambe et al., 2011; Trepat et al., 2009). We propose that p114 RhoGEF activates RhoA at AJs when epithelia move, perhaps as a mechanosensitive response to tugging forces transmitted from cellular tractions to AJs (Acharya et al., 2018). Junctional RhoA enhances contractile tension at the AJ, promoting an increase in tissue tension that is
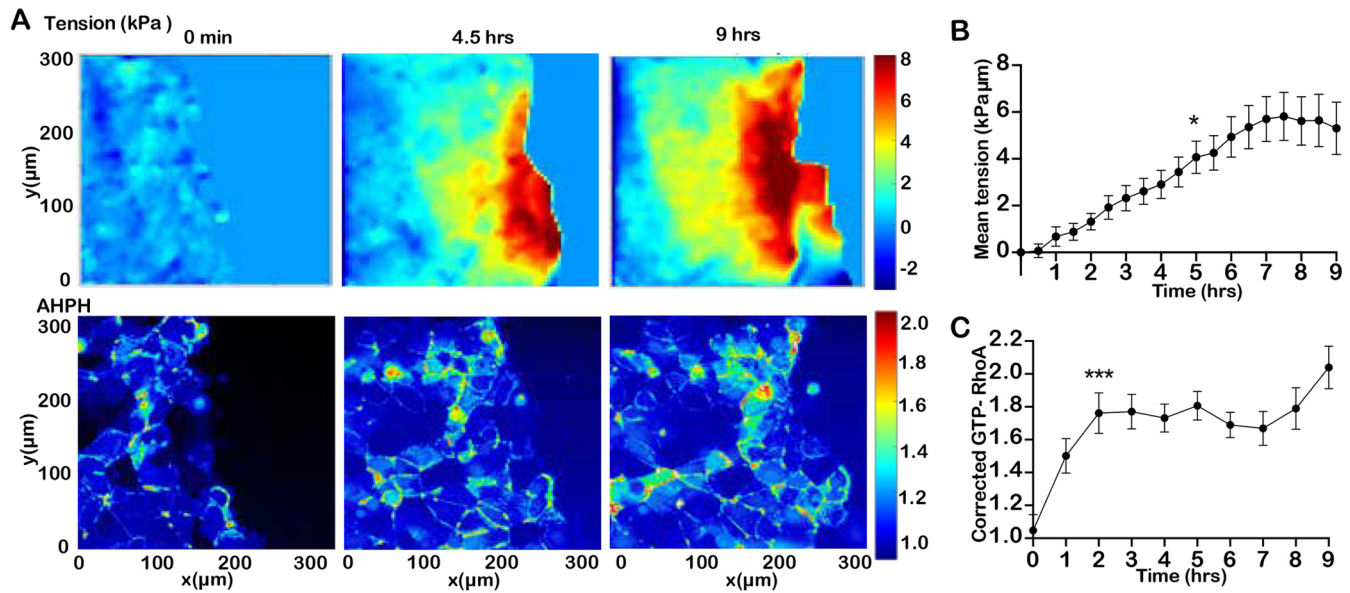
Fig. 3. Comparison of monolayer stress and GTP-RhoA levels during epithelial migration. (A–C) MCF-7 cells expressing GFP–AHPH were allowed to migrate on PDMS substrata for simultaneous capture of GTP-RhoA and traction force microscopy/BISM. (A) Representative stress maps (top) and GFP–AHPH images (bottom) at the indicated time points. Quantitation of (B) mean monolayer tension and (C) mean junctional GTP-RhoA levels (GFP–AHPH, corrected for cytosolic expression in each cell) within the field of view are shown. Note that the number of rows of cells in the field of view increases with migration. Data are means±s.d. n=3 independent experiments. *P<0.05; ***P<0.001. One-way ANOVA with Dunnett's multiple comparisons test.

accompanied by stabilization of E-cadherin and orderliness in collective migration. Elements in this system also have the capacity to introduce feedback into what may be initiated as a linear mechanotransduction pathway. For example, myosin II can initiate a positive feedback loop to promote stability of RhoA signalling itself (Priya et al., 2015). We also observed an apparent increase in active RhoA in a medial–apical pool, which could potentially exert tension on cell–cell junctions (Rauzi et al., 2010). Nonetheless, our anillin manipulation experiments indicate that there is a significant role for the junctional pool of GTP-RhoA. Thus, expressing AH–α-catenin in anillin-KD cells selectively restored GTP-RhoA to AJs and significantly restored junctional tension, E-cadherin stability and orderly migration to anillin-KD cells.

Stabilization of E-cadherin has the potential to reinforce AJs against pulling forces that they experience during migration (Acharya et al., 2018). A variety of mechanisms exist that can enhance cadherin adhesion when disruptive mechanical forces are applied (Charras and Yap, 2018; Rakshit et al., 2012). These include catch bonds found in the adhesive binding interaction (Rakshit et al., 2012) and in α-catenin binding to F-actin (Buckley et al., 2014; Ishiyama et al., 2018). The stabilization of E-cadherin by RhoA that we have now observed would provide an additional line of protection by increasing the levels of this adhesion receptor present at the AJ, thereby increasing the adhesion forces that resist detachment.

How junctional RhoA signalling serves to promote orderliness in cell migration is an interesting question for future studies. Anillin KD was associated with both an increase in the speed with which cells moved and a reduction in the organized fashion of migration. Both these features were restored by expression of AH–α-catenin, implicating a role for junctional RhoA signalling. This notion was supported by the effects of p114 RhoGEF KD, which caused similar changes in cell migration. One possibility is that loss of a junctional RhoA response promotes some features of epithelial–mesenchymal transformation, although E-cadherin levels were not compromised by anillin KD and cells retained cell–cell junctions as they moved.

Stabilization of E-cadherin at AJs might also antagonize a tendency for tissue fluidity to increase during migration (Tetley et al., 2019). Finally, Ozawa et al. (2020) have reported that cell–cell adhesion can dampen the generation of cryptic lamellipodia for epithelial migration. Clearly, our current observations open up rich possibilities for further analysis.

MATERIALS AND METHODS
Cell culture and transfection
MCF-7 cells (ATCC; identifier HTB-22) were maintained in Dulbecco's modified Eagle medium (DMEM, Gibco) supplemented with 10% FBS, 1% non-essential amino acids (NEAA), 1% L-glutamine (Gibco) and penicillin-streptomycin (Gibco). HEK-293T (ATCC; identifier CRL-3216) cells were maintained in DMEM supplemented with 10% FBS-HI (Thermo Fisher Scientific, Gibco), 1% NEAA, 1% L-glutamine and penicillin-streptomycin. Cell lines were maintained in 25 µg/ml plasmocin (InvivoGen) to prevent mycoplasma contamination and were routinely screened for the presence of mycoplasma. Barrier-separated cell monolayers were generated by seeding MCF-7 cells at a confluency of 1.5×10^5 cells/ml in two-well culture insertion barriers (ibidi), pre-placed in glass-bottom dishes (Shengyou Biotechnology). After 100% confluency was reached, the barriers were removed, and monolayer migration was monitored. For live-cell imaging, culture medium was replaced by Hank's balanced salt solution supplemented with 10% FBS, 10 mM HEPES (pH 7.4) and 5 mM $CaCl_2$. Transient transfections were performed after seeding using Lipofectamine 2000 or 3000 for DNA (Invitrogen) and RNAiMAX for RNA (Invitrogen). Mixtures were prepared according to the manufacturer's protocol.

Zebrafish husbandry and live imaging of epiboly migration
Adult zebrafish and embryos were maintained using standard protocols approved by the University of Queensland Animal Ethics Committee. Generation of the $tg(krt4:GFP-AHPH)$[uqay2] line was described recently (Duszyc et al., 2021). $Tg(krt4:GFP-AHPH)$[uqay2] fish were crossed to wild-type fish. Heterozygous transgenic 4.5 hours post fertilization (hpf) embryos were dechorionated using forceps and mounted in low-melting agarose (1% in E3 embryo medium; based on Cold Spring Harbor Protocols) in glass-bottom imaging dishes.
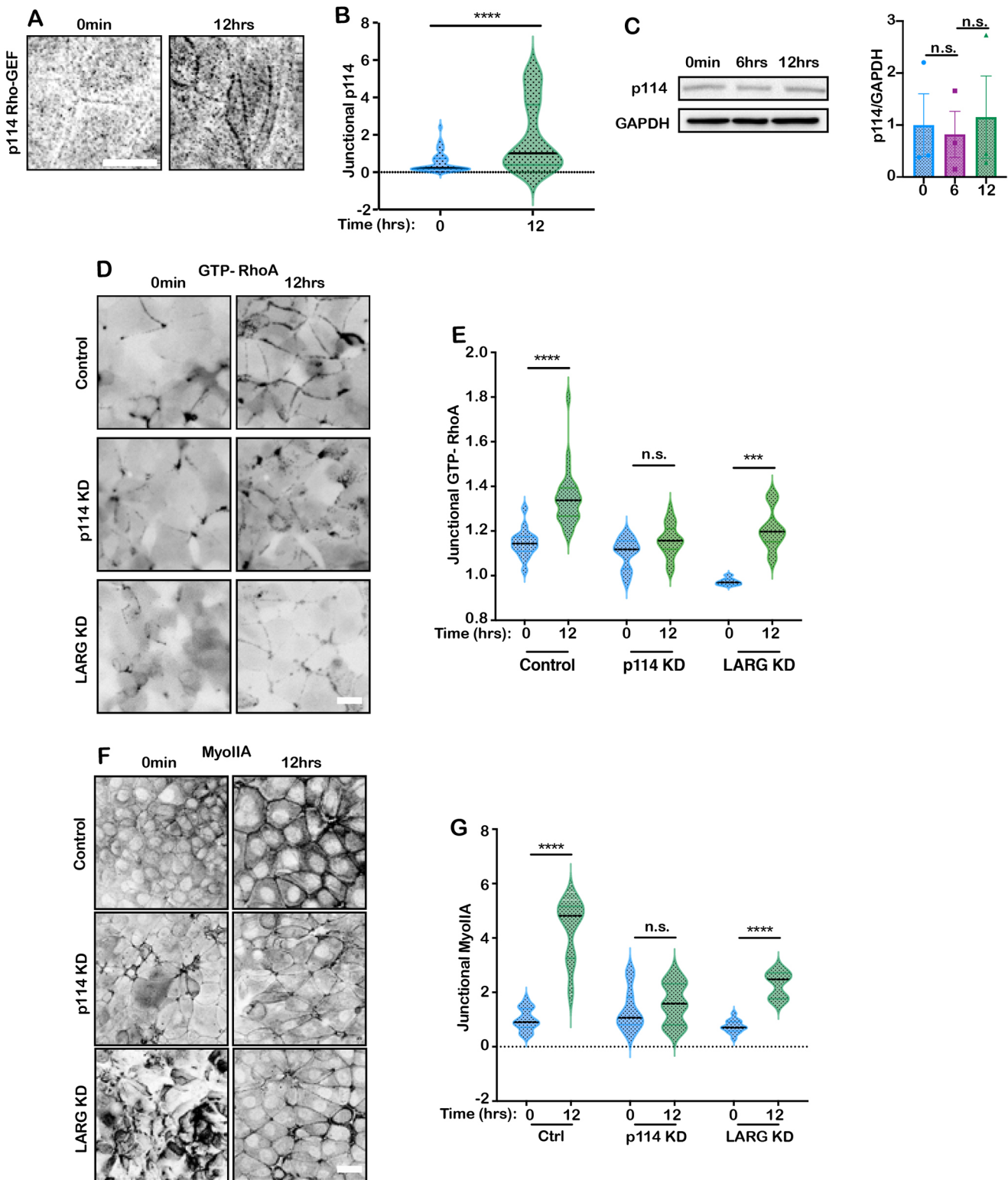
Fig. 4. p114 RhoGEF is required for enhanced RhoA signalling at AJs during epithelial migration. (A,B) Junctional p114 RhoGEF in migrating MCF-7 monolayers. Representative images (A) and quantification (B) at 0 h and 12 h of migration are shown. (C) Representative immunoblots (left) and quantification (right) of total p114 RhoGEF in migrating MCF-7 monolayers (0–12 h). GAPDH is shown as a loading control. (D–G) Effect of p114 RhoGEF KD on RhoA signalling at AJs in migrating MCF-7 monolayers. Monolayers were transfected with control siRNA (control, Ctrl), p114 RhoGEF siRNA (p114 KD) or LARG siRNA (LARG KD). Representative images and quantitation for GFP–AHPH (detecting GTP-RhoA; D,E) and NMIIA (MyoIIA; F,G) at 0 h and 12 h of migration are shown. Data for A,B,D–F were taken within the first seven rows of cells. In B,E,G, black lines show the mean. Data in C are mean±s.e.m. n=3 independent experiments (for B,E and G, each independent experiment contained 18–22 technical replicates). n.s., not significant; ***P<0.001; ****P<0.0009. Two-tailed unpaired t-test. Scale bars: 20 µm.
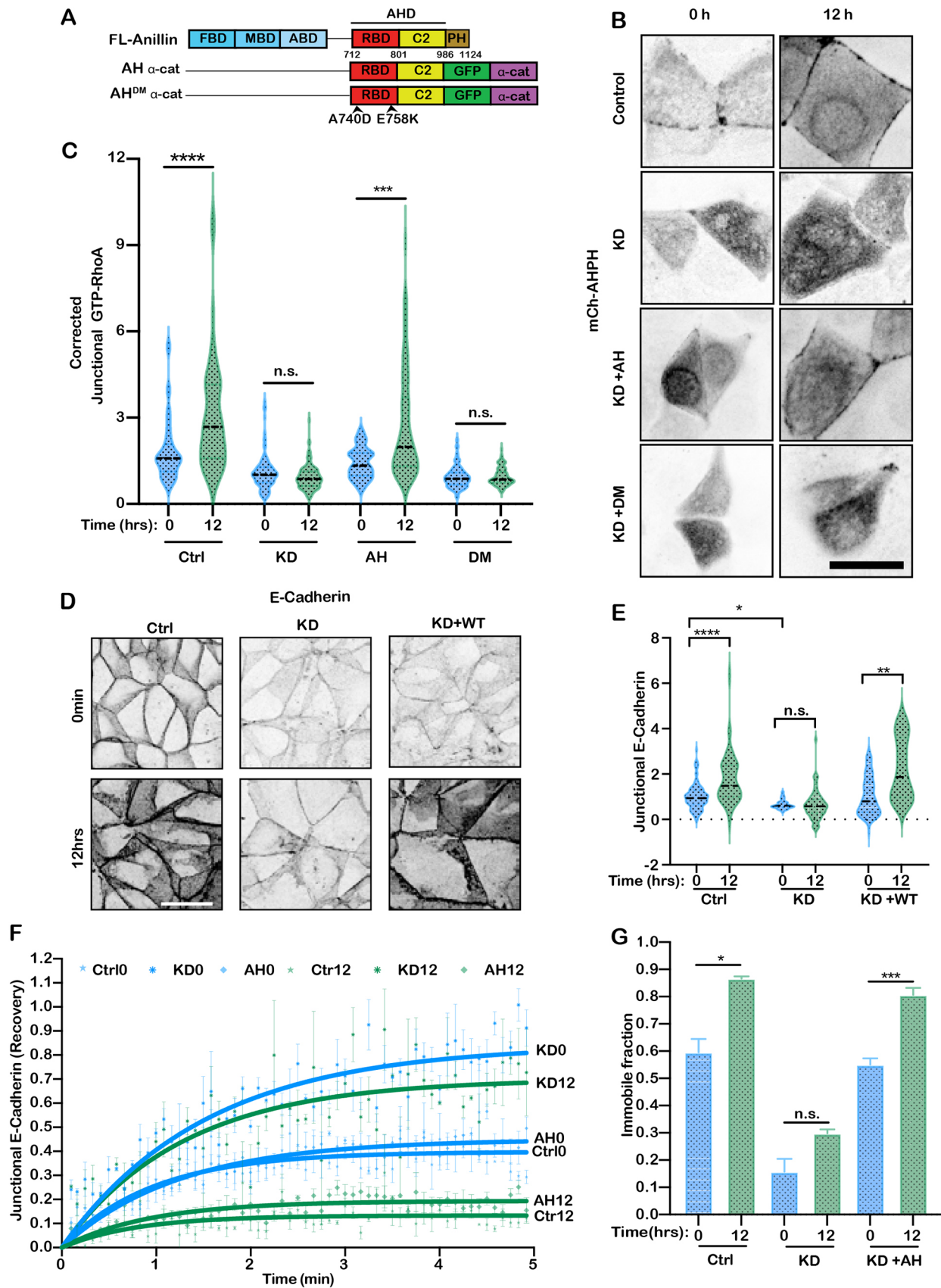
Fig. 5. See next page for legend.

Fig. 5. Junctional RhoA stabilizes E-cadherin in migrating monolayers.
RhoA was selectively restored at AJs by targeting the GTP-RhoA-binding domain of anillin (AHD) to E-cadherin in anillin KD cells. (A) The anillin AHD or its RhoA-uncoupled (DM) mutant were fused to GFP and the N terminus of α-catenin, as described in detail previously (Budnar et al., 2019), to give AH–α-catenin and AH^{DM}–α-catenin, respectively. Amino acid substitutions in the DM mutant are indicated. ABD, actin-binding domain; α-cat, α-catenin; C2, C2 domain; FBD, formin-binding domain; MBD, myosin-binding domain; PH, pleckstrin homology domain; RBD, Rho-binding domain. (B,C) Effect on junctional GTP-RhoA (detected using mCherry–AHPH) of expressing AH–α-catenin (AH) or AH^{DM}–α-catenin (DM) in anillin KD cells. Representative images (B) and quantification (C) are shown (Ctrl, control). (D,E) Impact of junctional RhoA signalling on E-cadherin levels at AJs in migrating MCF-7 monolayers. Representative immunofluorescence images (D) and quantification (E) are shown for control cells, anillin KD cells, and anillin KD cells expressing full-length anillin (KD+WT). (F,G) Effect of junctional RhoA signalling on fluorescence recovery of transiently-expressed E-cadherin–mCherry. FRAP curves (F) and immobile fractions (G) are shown for cells at 0 h and 12 h of migration. All data were collected from the first seven rows of cells. In C and E, black lines show the mean. Data in F and G are mean±s.e.m. n=3 independent experiments, each with 18–22 technical replicates. n.s., not significant; *P<0.05; **P<0.01; ***P<0.001; ****P<0.0009. Two-tailed, unpaired t-test. Scale bars: 20 µm.

Lentiviral infection
Lentivirus packaging was performed by Lipofectamine 2000-based co-transfection of HEK-293T cells with packaging vectors (VSV-G, RSV-rev, pRRE; Addgene Catalog number #12259, 12253, 12251) and the lentiviral vector pLL5.0 (gift from James Bear; Comprehensive Cancer Center, UNC, Chapel Hill, USA) containing the genes of interest in OptiMEM (Gibco). 8 h after transfection, the medium was replaced by normal culture medium. 10 mM sodium butyrate and fresh culture medium was added 24 h after transfection to reduce any pH changes. The virus-containing supernatant was subsequently harvested by centrifugation and concentrated on Millipore spin columns. Virus was stored at −80°C or used to infect target cells.

To infect target cells, concentrated virus was mixed with 8 µM polybrene and added to the cells. 24 h after infection, the medium was replaced by normal culture medium. The following constructs were expressed through lentiviral infections: GFP–AHPH (a gift from Michael Glotzer, University of Chicago, IL, USA), GFP alone, anillin KD, anillin KD with full-length anillin rescue (KD+WT), anillin KD with AH–GFP–α-catenin (AH–α-catenin) and anillin KD with AH^{DM}–GFP–α-catenin (AH^{DM}–α-catenin).

Immunofluorescence staining
For immunofluorescence staining, cells were cultured on glass coverslips and fixed with 4% paraformaldehyde (PFA; used for α-catenin, α-18, MRLC and pMRLC staining), 10% TCA (trichloroacetic acid; used for RhoA staining) or −20°C methanol (used for anillin, NMIIA, NMIIB, actin, E-cadherin and p114 RhoGEF staining) for 15 min. TCA fixation was terminated with 30 mM glycine in phosphate-buffered saline (PBS) for 5 min. After fixation, cells were permeabilized with 0.25% Triton X-100 for 5 min. Next, samples were blocked with 5% fat-free dry milk in PBS and subsequently incubated with primary antibodies overnight at 4°C and fluorescently labelled secondary antibodies for 2 h at room temperature. Finally, samples were washed and mounted in ProLong Gold (Cell Signaling Technology).

Western blotting
For western blotting, cells were lysed in 1× sample buffer (4×: 200 mM Tris-HCl, 40% glycerol, 8% SDS and 0.4% Bromophenol Blue) and incubated for 10 min at 100°C. Samples were run on 4, 8 or 15% SDS polyacrylamide electrophoresis gels (depending on the molecular weight of the proteins of interest) and transferred onto nitrocellulose membranes. The nitrocellulose membranes were subsequently blocked with 5% non-fat milk for 1 h, incubated with primary antibodies overnight at 4°C and incubated with species-specific horseradish peroxidase (HRP)-conjugated secondary antibodies for 1 h. Next, the membranes were developed using enhanced chemiluminescence (ECL).

Antibodies and chemicals
For immunofluorescence, mouse antibodies against the following proteins were used: MRLC (Abcam, ab594; 1:100), anillin (Santa Cruz Biotechnology, SC-271814; 1:100), myosin IIB (Abcam, ab684; 1:300), actin (Thermo Fisher Scientific, A5228; 1:100) and RhoA (Santa Cruz Biotechnology, SC-418; 1:100). Rabbit antibodies against the following proteins were used: α-catenin (Thermo Fisher Scientific, 711200; 1:100), pMRLC (Merck Millipore, AB3381; 1:50) and myosin IIA (Biolegend, 909801; 1:300). Rat antibodies against the following proteins were used: α-18 (a gift from Professor Akira Nagafuchi, Nara Medical University, Japan; 1:50) and rat E-cadherin (Abcam, 13-1800; 1:500). A goat antibody against p114 RhoGEF was purchased from Sapphire Bioscience (EB06163; 1:100). Alexa Fluor 488-, Alexa Fluor 547- and Alexa Fluor 647-conjugated antibodies against mouse, rabbit, rat and goat immunoglobulin were purchased from Thermo Fisher Scientific (1:500). Alexa Fluor 647-conjugated phalloidin was purchased from Thermo Fisher Scientific (A22287).

For western blotting, mouse antibodies against the following proteins were used: anillin (Santa Cruz Biotechnology, SC-271814; 1:200) and GFP (Sigma-Aldrich, 11874460001; 1:2000). Rabbit antibodies against the following proteins were used: GAPDH (Trevigen, 2275-PC-100; 1:5000), p114 RhoGEF (Abcam, ab96520; 1:100) and α-catenin (Thermo Fisher Scientific 711200; 1:500). HRP-conjugated antibodies against mouse and rabbit immunoglobulin were purchased from Bio-Rad Laboratories (1:5000).

DNA constructs and siRNAs
The following previously published DNA constructs were used in this study: pLL5.0-GFP (GFP alone), pLL5.0-anillin-shRNA (anillin KD) and pLL5.0-anillin-shRNA-GFP-anillin FL (KD+WT) (Budnar et al., 2019). pLL5.0 E-cadherin–mCherry KDR has also been published previously (Wu et al., 2015). pLL5.0-anillin-shRNA-CMV-AHPH-GFP-α-cat FL (anillin KD with AH–α-catenin) and pLL5.0-anillin-shRNA-CMV-AHPH^{DM}-GFP-α-cat FL (anillin KD with AH^{DM}–α-catenin) were cloned for this study. DNA maps are available upon request.

The following siRNAs were used for transient gene silencing: anillin, 5′-ATGCCTCTTTGAATAAATT-3′ (sense) and 5′-TTTATTCAAAGAGG-CATCG-3′ (antisense); p114 RhoGEF A, 5′-TCAGGCGCTTGAAAGA-TATT-3′ (sense) and 5′-TATCTTTCAAGCGCCTGATG-3′ (antisense); p114 RhoGEF B, 5′-GGACGCAACTCGGACCAATTT-3′ (sense) and 5′-ATTGGTCCGAGTTGCGTCCCA-3′ (antisense); LARG A, 5′-GGCAA-CATTTCCCAAGATATT-3′ (sense) and 5′-TATCTTGGGAAATGTTGC-CAG-3′ (antisense); LARG B, 5′-GATCAAATCTCGTCAGAAATT-3′ (sense) and 5′-TTTCTGACGAGATTTGATCAT-3′ (antisense). All siRNAs were purchased from Sigma-Aldrich.

Traction force microscopy sample preparation
Polyacrylamide gels with a Young's modulus of 15 kPa were prepared using CY-52-276 A and CY-52-276 B (Dow Corning Toray) in 1:1 v/v ratio. Gels were spin coated at 500 g for 30 s to get an even coating and cured for 2 h at 80°C. 5% (3-aminopropyl)triethoxysilane (APTES; Sigma-Aldrich, A3648) in ethanol was added to the gels followed by an incubation of 10 min. The solution was then removed, and the gels were washed with ethanol and dried at 80°C for 30 min. 200 nm nanobeads (Thermo Fisher Scientific, FluoSpheres) were diluted at 1:30,000 with distilled water and sonicated for 10 min to break the clumps. The silane–PDMS was functionalized with the nanobeads solution for 5 min at room temperature, after which the beads were removed again. Functionalized gels were rinsed with distilled water and dried for 15 min at 80°C. Beads were then passivated with 100 mM Tris for 10 min at room temperature. Subsequently, the solution was removed, gels were washed with distilled water and dried in an oven for 15 min at 80°C. 10 µg/ml fibronectin was added to the gels followed by 1 h incubation at room temperature. Next, the gels were incubated with 1% Pluronic (Sigma-Aldrich, Product Number P2443) for 30 min to sterilize and were then washed with PBS. Finally, cells were added and monitored until a confluent monolayer was generated.

Microscopy and image analysis
The following microscopes were used in this study: (1) Traction force microscopy experiments were performed on a Nikon Ti-E deconvolutional
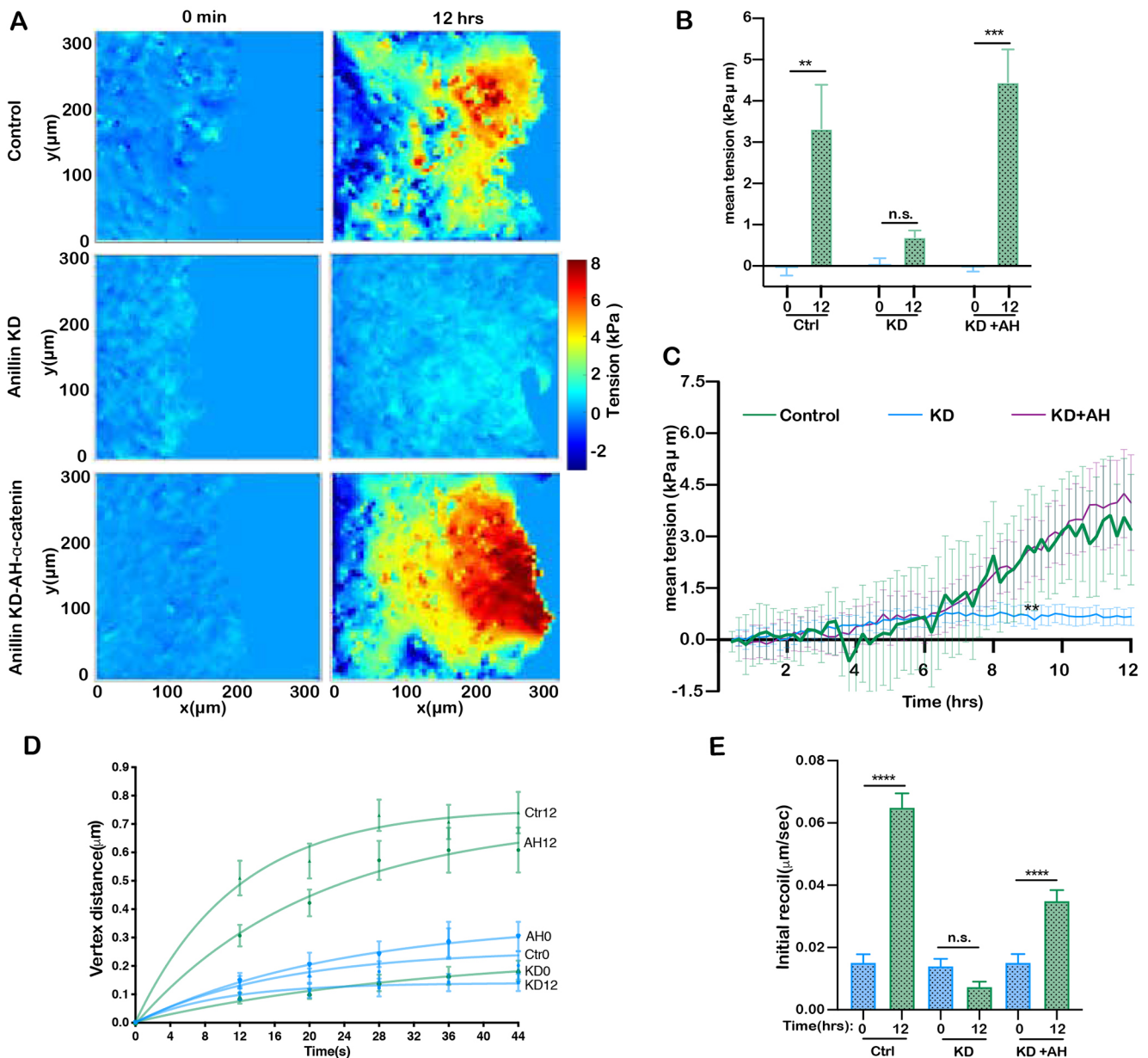
Fig. 6. Junctional RhoA increases monolayer tension during epithelial migration. Monolayer stress (BISM; A–C) or AJ recoil (D,E) were measured in control cells (Ctrl), anillin KD cells (KD) or anillin KD cells reconstituted with AH–α-catenin (KD+AH) during cell migration. BISM experiments were performed in cells grown on PDMS substrata, whereas cells for recoil studies were grown on glass. (A) Representative stress maps at 0 h and 12 h of migration are shown. (B,C) Quantitation of monolayer stress was performed for the whole field of view. (D,E) Recoil experiments were performed on cells within the first seven rows from the migration front, and recoil curves for (D) and initial recoil (E) were measured for cells at 0 h and 12 h of migration. Data are mean±s.e.m. n=3 independent experiments (for D and E, each independent experiment contained 15–22 technical replicates). n.s., not significant; **$P<0.01$; ***$P<0.001$; ****$P<0.0009$. Two-tailed, unpaired t-test (B,E) or one-way ANOVA with Dunnett's multiple comparisons test (C).

microscope (20×, 0.75 NA Plan Apo objective) driven using NIS Elements AR software. (2) Laser ablation experiments were performed on a Zeiss LSM 510 Meta confocal microscope (63×, 1.4 NA Plan Apo objective) driven using Zen Black software. (3) FRAP experiments were performed on an inverted Zeiss LSM 510 Meta confocal microscope (100×, 1.4 NA Plan Apo objective) driven using Zen Black software. (4) FRET experiments were performed on a Zeiss LSM 710 Meta confocal microscope (63×, 1.4 NA Plan Apo objective) with specific detector for CFP/YFP imaging. The microscope was driven using Zen Black software. (5) Immunofluorescence images were acquired with an inverted Zeiss 880 or an upright 710 Meta laser-scanning microscope (63×, 1.4 NA Plan Apo objective; or 100×, 1.4 NA Plan Apo objective) driven using Zen Black software. (6) Zebrafish were imaged on a Zeiss LSM710 confocal microscope (20×, 0.8NA Plan Apo objective).

Traction force microscopy and stress analysis

Cells were observed using brightfield microscopy. Nanobeads were observed using the far-red channel. At the end of the experiment, cells were trypsinized to obtain null-force observations. The gel deformations were obtained by recording the displacement of nanobeads in comparison to the null-force images. For particle image velocimetry (PIV), the PIVlab toolbox (MATLAB) was used to obtain velocity vectors by saving images in the sequence (1–2, 3–4, 5–6,…) and not (1–2, 2–3, 3–4,…). When acquiring movies using a 20× objective, three pass filters were used: 128(64), 64(32), 32(16) pixels. After PIV, outliers were removed manually. Vector validation was conducted by defining, and then refining, velocity limits. BISM (Bayesian inversion stress microscopy) was run to back calculate the internal stress field of a cell monolayer from the traction forces
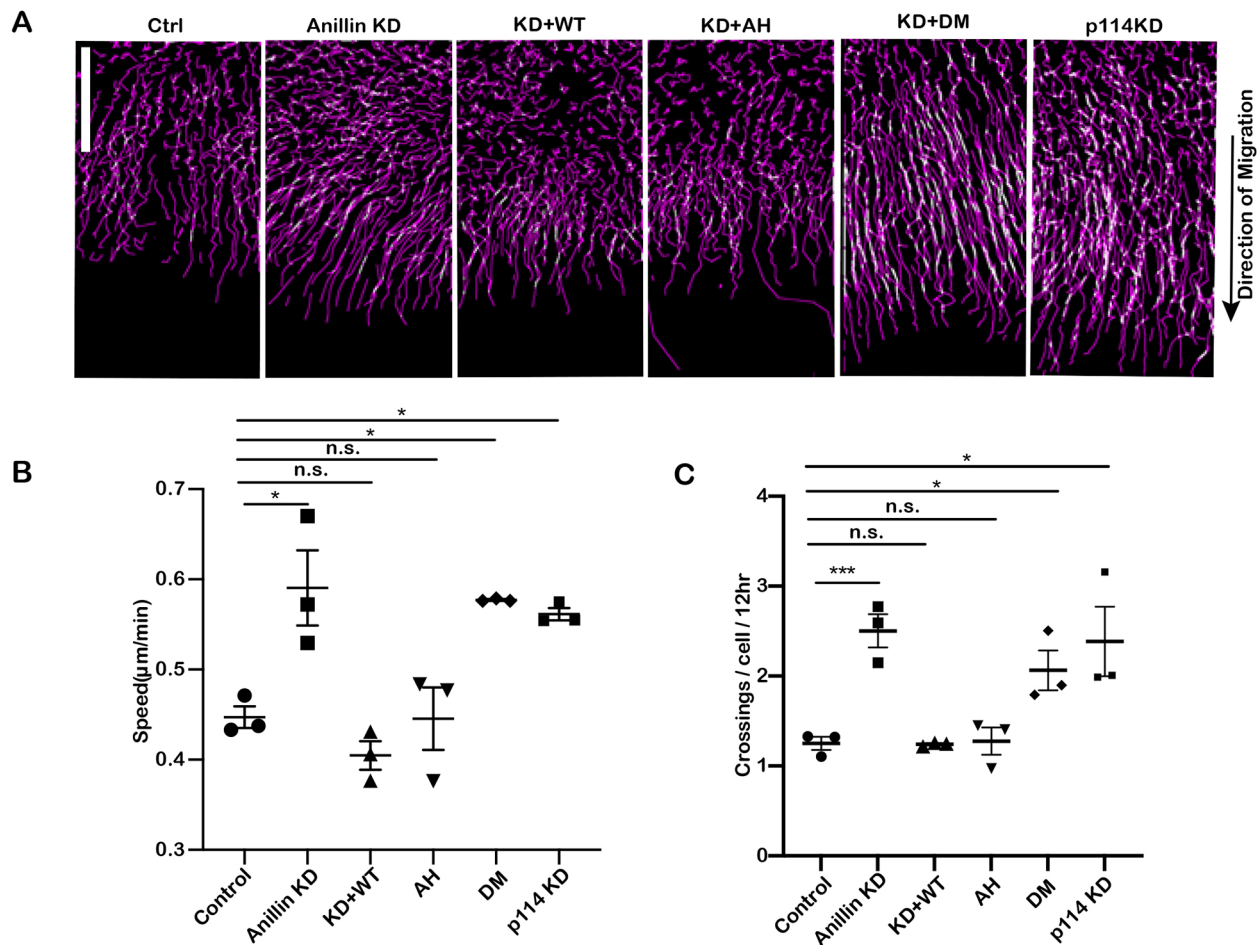
Fig. 7. Junctional RhoA influences the speed and orderliness of epithelial migration. (A–C) Migrating MCF-7 cells were monitored for 12 h by tracking their nuclei labelled with Hoechst 33342 dye. Control cells (Ctrl) were compared to anillin KD cells, anillin KD cells expressing either full-length anillin (KD+WT), AH–α-catenin (KD+AH) or AH^{DM}–α-catenin (KD+DM), or to p114 RhoGEF KD cells (p114KD). Representative tracks (magenta) and crossing events (white) are shown (A), with quantitation of cell speed (B) and the number of times that the track for a cell crossed that of another cell in the 12 h experiment (C). Each individual data point represents the mean of a movie, each comprising ∼400 individual tracks. Data are mean±s.e.m. from n=3 independent experiments. n.s., not significant; *P<0.05; ***P<0.001. One-way ANOVA with Dunnett's multiple comparisons test.

data. For this, we analysed regions of 300 μm×300 μm, applying stress-free boundary conditions only on the cell-free boundary (on the right-hand side of Fig. 1A). As in Ollech et al. (2020), we validated BISM used with these boundary conditions by comparing tension values obtained by spatially-averaging the two-dimensional tension field over the direction parallel to the migrating front, with the one-dimensional tension obtained from direct integration of traction forces along the direction perpendicular to the migrating front (Trepat et al., 2009) (data not shown). Images in Fig. 1A,B show isotropic stress (or tension) spatial patterns derived from a representative movie. For statistical comparison we then derived the mean of time-averaged stress for the analysed region. Average isotropic stress values correspond to a subregion in bulk, away from boundaries. The MATLAB code for BISM tissue level tension analysis is available on github (https://github.com/shef552/Traction-Force-Microscopy-and-Stress-analysis-code.git).

Two-photon laser ablation

Junctional tension of monolayers was examined by measuring the recoil of vertices after laser ablation of AJs marked by E-cadherin–mCherry, as previously described (Liang et al., 2016). A region of constant area (3.8×0.6 μm, with the longer axis orthogonal to the junctions) of the apical junctions was ablated by a femtosecond infrared two-photon 790 nm laser with 20% transmission and 15 iterations. The amount of recoil after ablation (ε) was measured as the change in the distance L between the vertices at t=t

with respect to t=0 [i.e. $L(t)-L(0)$] of the ablated contacts as a function of time (t). At least 15 junctions were ablated and quantified for each condition of every experiment and the mean values of $\varepsilon(t)$ were plotted against time to determine the extent of junctional initial recoil velocity after ablation using non-linear regression.

Tracking cell motion and crossing analysis

Confluent monolayers of MCF-7 cells were imaged using nuclear staining after removing the culture insertion barriers. Cell nuclei were stained with a blue fluorescent dye (Hoechst 33342, a counter stain for viable cells that emits fluorescence when bound to DNA) and imaged for 12 h at 12 min intervals. The nuclei were tracked using Imaris, and images were analysed with customized code (available on request) that used x coordinates, y coordinates and intensities of particles to measure the crossing events.

RhoA FRET

FRET measurements and analysis were performed 48 h after transfection with pTriEx-RhoA FRET WT biosensor (Addgene plasmid #12150). Imaging was performed on an LSM710 Zeiss confocal microscope. The donor channel was acquired using a 458 nm laser line and emission was collected in the donor emission region (470–490 nm). The acceptor channel was acquired using a 514 nm laser line and emission was collected in the acceptor emission range (530–590 nm). FRET signal was acquired using a

458 nm laser line and emission was collected in the acceptor emission range (530–590 nm). RhoA activation images were generated by calculating FRET:CFP emission ratios.

FRAP

FRAP measurements and analysis were performed 36 h after transfection with E-cadherin–mCherry. A region of interest (ROI) in the centre of cell–cell contacts was bleached using a 790 nm laser followed by 5 min of imaging with a frame interval of 1 s. To generate FRAP profiles, mean grey values at the bleached ROIs were measured during the recovery phase. The mean grey values obtained from the bleached region were normalized to the average pre-bleach value and fitted to a one-phase exponential association function using GraphPad Prism software.

Junctional protein quantification

Junctional intensity of E-cadherin, NMIIA, NMIIB, F-actin, α-catenin and α-18 was quantified by generating line scans of 20 μm lines perpendicular to randomly selected junctions. Line pixel intensities were then fitted with a Gaussian curve, and peak values were obtained from the fitting. Pixel intensity values of 10 pixels on either side of the centres were considered background and subtracted from the peak values. Due to heterogenous expression levels of GFP–AHPH, the pixel values of 10 pixels on either side of the centres were divided from the peak values. A minimum of 60 junctions were measured in each experimental condition. The relative values of experimental conditions were normalized to the value of control cells for comparison.

Statistical analysis

Statistical significance of the data was analysed by calculating P values using two-tailed Student's t-tests or one-way ANOVA tests with Dunnett's multiple comparison test. Statistical analysis is shown as follows: n.s., not significant; $*P<0.05$; $**P<0.01$; $***P<0.001$; $****P<0.0009$.

Competing interests
The authors declare no competing or financial interests.

Author contributions
Conceptualization: S.G., S.B., G.A.G., A.S.Y.; Methodology: S.G., S.V., X.L., P.M., I.N.; Software: S.G.; Validation: S.G.; Formal analysis: S.G.; Investigation: I.N., A.S.Y.; Resources: S.G., S.B., A.S.Y.; Data curation: S.G., K.D., I.N.; Writing - original draft: S.G., A.S.Y.; Visualization: S.G.; Supervision: S.B., G.A.G., A.S.Y.; Project administration: A.S.Y.; Funding acquisition: A.S.Y.

Peer review history
The peer review history is available online at https://journals.biologists.com/jcs/article-lookup/doi/10.1242/jcs.258767

References
Acharya, B. R., Wu, S. K., Lieu, Z. Z., Parton, R. G., Grill, S. W., Bershadsky, A. D., Gomez, G. A. and Yap, A. S. (2017). Mammalian diaphanous 1 mediates a pathway for E-cadherin to stabilize epithelial barriers through junctional contractility. *Cell Rep.* **18**, 2854-2867. doi:10.1016/j.celrep.2017.02.078

Acharya, B. R., Nestor-Bergmann, A., Liang, X., Gupta, S., Duszyc, K., Gauquelin, E., Gomez, G. A., Budnar, S., Marcq, P., Jensen, O. E. et al.

(2018). A mechanosensitive RhoA pathway that protects epithelia against acute tensile stress. *Dev. Cell* **47**, 439-452.e6. doi:10.1016/j.devcel.2018.09.016

Bruce, A. E. E. and Heisenberg, C.-P. (2020). Mechanisms of zebrafish epiboly: a current view. *Curr. Top. Dev. Biol.* **136**, 319-341. doi:10.1016/bs.ctdb.2019.07.001

Buckley, C. D., Tan, J., Anderson, K. L., Hanein, D., Volkmann, N., Weis, W. I., Nelson, W. J. and Dunn, A. R. (2014). The minimal cadherin-catenin complex binds to actin filaments under force. *Science* **346**, 1254211. doi:10.1126/science.1254211

Budnar, S., Husain, K. B., Gomez, G. A., Naghibosadat, M., Varma, A., Verma, S., Hamilton, N. A., Morris, R. G. and Yap, A. S. (2019). Anillin promotes cell contractility by cyclic resetting of RhoA residence kinetics. *Dev. Cell* **49**, 894-906.e12. doi:10.1016/j.devcel.2019.04.031

Cavanaugh, K. E., Staddon, M. F., Munro, E., Banerjee, S. and Gardel, M. L. (2020). RhoA mediates epithelial cell shape changes via mechanosensitive endocytosis. *Dev. Cell* **52**, 152-166.e5. doi:10.1016/j.devcel.2019.12.002

Charras, G. and Yap, A. S. (2018). Tensile forces and mechanotransduction at cell-cell junctions. *Curr. Biol.* **28**, R445-R457. doi:10.1016/j.cub.2018.02.003

Curran, S., Strandkvist, C., Bathmann, J., de Gennes, M., Kabla, A., Salbreux, G. and Baum, B. (2017). Myosin II controls junction fluctuations to guide epithelial tissue ordering. *Dev. Cell* **43**, 480-492.e6. doi:10.1016/j.devcel.2017.09.018

Duszyc, K., Gomez, G. A., Lagendijk, A. K., Yau, M.-K., Nanavati, B. N., Gliddon, B. L., Hall, T. E., Verma, S., Hogan, B. M., Pitson, S. M. et al. (2021). Mechanotransduction activates RhoA in the neighbors of apoptotic epithelial cells to engage apical extrusion. *Curr. Biol.* **31**, 1326-1336.e5. doi:10.1016/j.cub.2021.01.003

Friedl, P. and Gilmour, D. (2009). Collective cell migration in morphogenesis, regeneration and cancer. *Nat. Rev. Mol. Cell Biol.* **10**, 445-457. doi:10.1038/nrm2720

Friedl, P. and Mayor, R. (2017). Tuning collective cell migration by cell-cell junction regulation. *Cold Spring Harb. Perspect. Biol.* **9**, a029199. doi:10.1101/cshperspect.a029199

Garcia De Las Bayonas, A., Philippe, J.-M., Lellouch, A. C. and Lecuit, T. (2019). Distinct RhoGEFs activate apical and junctional contractility under control of G proteins during epithelial morphogenesis. *Curr. Biol.* **29**, 3370-3385.e7. doi:10.1016/j.cub.2019.08.017

Guilluy, C., Swaminathan, V., Garcia-Mata, R., O'Brien, E. T., Superfine, R. and Burridge, K. (2011). The Rho GEFs LARG and GEF-H1 regulate the mechanical response to force on integrins. *Nat. Cell Biol.* **13**, 722-727. doi:10.1038/ncb2254

Ishiyama, N., Sarpal, R., Wood, M. N., Barrick, S. K., Nishikawa, T., Hayashi, H., Kobb, A. B., Flozak, A. S., Yemelyanov, A., Fernandez-Gonzalez, R. et al. (2018). Force-dependent allostery of the α-catenin actin-binding domain controls adherens junction dynamics and functions. *Nat. Commun.* **9**, 5121. doi:10.1038/s41467-018-07481-7

Kelly, P., Casey, P. J. and Meigs, T. E. (2007). Biologic functions of the G12 subfamily of heterotrimeric g proteins: growth, migration, and metastasis. *Biochemistry* **46**, 6677-6687. doi:10.1021/bi700235f

Lecuit, T. and Yap, A. S. (2015). E-cadherin junctions as active mechanical integrators in tissue dynamics. *Nat. Cell Biol.* **17**, 533-539. doi:10.1038/ncb3136

Liang, X., Michael, M. and Gomez, G. A. (2016). Measurement of mechanical tension at cell-cell junctions using two-photon laser ablation. *Bio Protoc.* **6**, e2068. doi:10.21769/BioProtoc.2068

Nier, V., Jain, S., Lim, C. T., Ishihara, S., Ladoux, B. and Marcq, P. (2016). Inference of internal stress in a cell monolayer. *Biophys. J.* **110**, 1625-1635. doi:10.1016/j.bpj.2016.03.002

Ollech, D., Pflästerer, T., Shellard, A., Zambarda, C., Spatz, J. P., Marcq, P., Mayor, R., Wombacher, R. and Cavalcanti-Adam, E. A. (2020). An optochemical tool for light-induced dissociation of adherens junctions to control mechanical coupling between cells. *Nat. Commun.* **11**, 472. doi:10.1038/s41467-020-14390-1

Ozawa, M., Hiver, S., Yamamoto, T., Shibata, T., Upadhyayula, S., Mimori-Kiyosue, Y. and Takeichi, M. (2020). Adherens junction regulates cryptic lamellipodia formation for epithelial cell migration. *J. Cell Biol.* **219**, e202006196. doi:10.1083/jcb.202006196

Piekny, A. J. and Glotzer, M. (2008). Anillin is a scaffold protein that links RhoA, actin, and myosin during cytokinesis. *Curr. Biol.* **18**, 30-36. doi:10.1016/j.cub.2007.11.068

Priya, R., Yap, A. S. and Gomez, G. A. (2013). E-cadherin supports steady-state Rho signaling at the epithelial zonula adherens. *Differentiation* **86**, 133-140. doi:10.1016/j.diff.2013.01.002

Priya, R., Gomez, G. A., Budnar, S., Verma, S., Cox, H. L., Hamilton, N. A. and Yap, A. S. (2015). Feedback regulation through myosin II confers robustness on RhoA signalling at E-cadherin junctions. *Nat. Cell Biol.* **17**, 1282-1293. doi:10.1038/ncb3239

Rakshit, S., Zhang, Y., Manibog, K., Shafraz, O. and Sivasankar, S. (2012). Ideal, catch, and slip bonds in cadherin adhesion. *Proc. Natl. Acad .Sci. USA* **109**, 18815-18820. doi:10.1073/pnas.1208349109

Ratheesh, A., Gomez, G. A., Priya, R., Verma, S., Kovacs, E. M., Jiang, K., Brown, N. H., Akhmanova, A., Stehbens, S. J. and Yap, A. S. (2012).

Centralspindlin and α-catenin regulate Rho signalling at the epithelial zonula adherens. *Nat. Cell Biol.* **14**, 818-828. doi:10.1038/ncb2532

Rauzi, M., Lenne, P.-F. and Lecuit, T. (2010). Planar polarized actomyosin contractile flows control epithelial junction remodelling. *Nature* **468**, 1110-1114. doi:10.1038/nature09566

Reffay, M., Parrini, M. C., Cochet-Escartin, O., Ladoux, B., Buguin, A., Coscoy, S., Amblard, F., Camonis, J. and Silberzan, P. (2014). Interplay of RhoA and mechanical forces in collective cell migration driven by leader cells. *Nat. Cell Biol.* **16**, 217-223. doi:10.1038/ncb2917

Smutny, M., Cox, H. L., Leerberg, J. M., Kovacs, E. M., Conti, M. A., Ferguson, C., Hamilton, N. A., Parton, R. G., Adelstein, R. S. and Yap, A. S. (2010). Myosin II isoforms identify distinct functional modules that support integrity of the epithelial zonula adherens. *Nat. Cell Biol.* **12**, 696-702. doi:10.1038/ncb2072

Tambe, D. T., Hardin, C. C., Angelini, T. E., Rajendran, K., Park, C. Y., Serra-Picamal, X., Zhou, E. H., Zaman, M. H., Butler, J. P., Weitz, D. A. et al. (2011). Collective cell guidance by cooperative intercellular forces. *Nat. Mater.* **10**, 469-475. doi:10.1038/nmat3025

Terry, S. J., Zihni, C., Elbediwy, A., Vitiello, E., Leefa Chong San, I. V., Balda, M. S. and Matter, K. (2011). Spatially restricted activation of RhoA signalling at epithelial junctions by p114RhoGEF drives junction formation and morphogenesis. *Nat. Cell Biol.* **13**, 159-166. doi:10.1038/ncb2156

Tetley, R. J., Staddon, M. F., Heller, D., Hoppe, A., Banerjee, S. and Mao, Y. (2019). Tissue fluidity promotes epithelial wound healing. *Nat. Phys.* **15**, 1195-1203. doi:10.1038/s41567-019-0618-1

Trepat, X. and Fredberg, J. J. (2011). Plithotaxis and emergent dynamics in collective cellular migration. *Trends Cell Biol.* **21**, 638-646. doi:10.1016/j.tcb.2011.06.006

Trepat, X., Wasserman, M. R., Angelini, T. E., Millet, E., Weitz, D. A., Butler, J. P. and Fredberg, J. J. (2009). Physical forces during collective cell migration. *Nat. Phys.* **5**, 426-430. doi:10.1038/nphys1269

Wu, S. K., Lagendijk, A. K., Hogan, B. M., Gomez, G. A. and Yap, A. S. (2009). Active contractility at E-cadherin junctions and its implications for cell extrusion in cancer. *Cell Cycle* **14**, 315-322. doi:10.4161/15384101.2014.989127

Yonemura, S., Wada, Y., Watanabe, T., Nagafuchi, A. and Shibata, M. (2010). α-Catenin as a tension transducer that induces adherens junction development. *Nat. Cell Biol.* **12**, 533-542. doi:10.1038/ncb2055